

Todo list

ich glaub, das ist bullshit	2
der satz muss noch einmassiert werden	2
put in correct numbers	13
warum schaut das spectrum anders aus als das, was einzeln geplottet ist?	15
cps zu a.u. aendern	29
zahlen fuer sat eintragen	29
put in pictures for fdtd results and reference them	30

Contents

Table of Contents	i
List of Figures	i
List of Tables	ii
1 Coupling of Nanodiamonds to Photonic Structures	1
1.1 Additional Experimental Methods	2
1.1.1 Nano-manipulator	3
1.1.2 Determination of The Position of Nanodiamonds	4
1.1.3 The Pick-And-Place Process	6
1.2 Coupling SiV centers to Vertical-Cavity Surface Emitting Lasers	8
1.2.1 Vertical-Cavity Surface Emitting Lasers	8
1.2.2 SiV center in a Vertical-Cavity Surface Emitting Laser	9
1.3 Coupling Nanodiamonds to Optical Antennas	16
1.3.1 Plasmonic Antennas	16
1.3.2 Plasmonic Antenna Design and Simulation	19
1.3.3 SiV center in a Plasmonic Double Bowtie Antenna	21

List of Figures

1.1	Nano-manipulator in a SEM setup	3
1.2	Detail of nano-manipulator tips	4
1.3	Cross markers assisting identification of nanodiamonds	5
1.4	Combining fluorescence light and laser scanning microscope to identify nanodiamonds	6
1.5	Sketch of the pick-and-place process	6
1.6	Nano-manipulator carrying a nanodiamond	7
1.7	Sketch of a vertical-cavity surface emitting laser	9
1.8	SEM image of an array of VCSELs	10
1.9	Emission spectra and optical power of VCSEL Bm4	11
1.10	Scans of VCSELs with and without SiV center	12
1.11	SiV center properties before and after pick-and-place	13
1.12	Comparison of intensities between VCSEL Bm4 and VCSEL Bm2 . . .	13
1.13	Comparison of spectra between VCSEL Bm4 and VCSEL Bm2	14
1.14	Reflectivity of VCSEL Bm4	15
1.15	Schematic of a double bowtie antenna	17
1.16	Hot-spot of a double bowtie antenna	18
1.17	SEM images of double bowtie structures.	19
1.18	Simulation of the resonance spectrum of a double bowtie antenna . .	20
1.19	Localizing suitable nanodiamonds	22
1.20	Properties of a nanodiamond containing an ensemble of SiV centers .	23
1.21	Pick-and-place coupling of nanodiamond to antenna	24
1.22	Confocal scan of a gold double bowtie antenna	25
1.23	Spectra of a nanodiamond coupled to an antenna	26
1.24	Spectrum of a double bowtie antenna without nanodiamond	26
1.25	Properties of a nanodiamond containing a few SiV centers	29
1.26	Spectrum of preselected nanodiamond containing few SiV centers . .	29
1.27	Background-corrected spectrum of a nanodiamond in an antenna . .	30

List of Tables

--

Chapter 1

Coupling of Nanodiamonds to Photonic Structures

In the previous chapter, we reported on photoluminescence properties of different sets of SiV centers. Across the available samples, emitters were found to exhibit considerable variations in wavelength, linewidth as well as intensity of zero-phonon-lines. This broad variety in combination with the ability to examine SiV centers individually opens up the possibility to preselect emitters according to desired spectroscopic parameters, such as narrow linewidths, high count-rates and single photon emission.

Once suitable emitters are identified, their host nanodiamonds can be moved with precision using pick-and-place methods. In particular, SiV centers may be transferred and coupled to photonic structures where their extraordinary properties can be exploited to create single photon source. Such sources are useful tools, widely required for applications in metrology and various quantum technologies such as quantum computing or quantum cryptography.

In the scope of this thesis, nanodiamonds including suitable SiV centers were identified and coupled to two different kinds of structures: Vertical-Cavity Surface Emitting Lasers (VCSELs) and plasmonic nano-antennas.

To create a hybrid-integrated single photon source, a nanodiamond containing an SiV center placed on top of a VCSEL. The SiV center is positioned such that it is directly pumped by the VCSEL output laser beam. Thus, the emission of the SiV center is steered indirectly via the operation of the VCSEL. Through the use of suitable optical filters allowing only SiV center fluorescence light to emerge, a controlled single photon source can be realized. This system is interesting in the context of metrological applications, as it constitutes a promising building block for a portable device ready to calibrate single photon detectors.

Coupling SiV centers to plasmonic nano-antennas aims at enhancing the detectable photoluminescence intensity of an emitter. As described in previous chapters, not only ZPL position and linewidth, but also the photoluminescence intensity varies strongly

among individual SiV centers. Obtaining a single photon source with a photon flux rate large enough to reliably and precisely be measured by a low photon flux detector is a key requirement for applications in metrology [?]. Furthermore, plasmonic antennas can be used to tune the emitters' photoluminescence spectrum.

1.1 Additional Experimental Methods

Coupling SiV centers to photonic structures requires specialized experimental methods. A range of challenges must be overcome: First, additionally to the spectroscopic preselection, the pick-and-place process poses further technical restrictions on the suitability of a host nanodiamond. The size of the host nanodiamond has to be bigger than 70 nm and they have to lie isolated on the substrate surface, i.e. with a distance of about one micrometer. This substantially reduces the number of SiV center candidates ready to be coupled to photonic structures. Another challenge is posed by accurately picking up a single nanodiamond hosting an SiV center and placing it precisely at a specified position within a given photonic structure. Furthermore, since the SiV center is to function as the photoluminescence emitter, it must not be damaged during the relocation process. To minimize both the damage cause by electron radiation, both the dose and the energy are minimized. Hence, the pick-and-place process is performed as fast as possible and with a low acceleration voltage that is just strong enough to see a hazy image of the nanodiamond.

In the context of this thesis we explored the following methods to couple nanodiamonds to photonic structures:

1. Directly spin-coat the target structures with a nanodiamond solution and consecutively look for a structure containing a nanodiamond with an SiV center exhibiting the desired spectroscopic properties. Frankly, this method relies on chance and is only feasible for the application with antenna structures due to the large number of antennas on one substrate. It is not advised to be used with VCSELs because of their morphology and the small number of VCSELs on an individual piece of substrate.
2. Identify nanodiamonds containing suitable SiV centers and individually relocate them to the destination structure using the tip in a scanning electron microscopy to perform a pick-and-place routine. For this method to be effective, nanodiamonds must have a certain size. The obvious advantage of this method is the fact that only the very best emitters are used. Furthermore, the pick-and-place process can be monitored in real-time. On the other hand, the electron radiation present during the pick-and-place process may damage the SiV center, introducing a risk of completely invalidating an emitter.
3. Identify nanodiamonds containing suitable SiV centers and individually relocate them to the destination structure using an atomic force microscope to perform a pick-and-place routine. While this method has the advantage that the nan-

odiamonds are not irradiated with electrons, the disadvantage is that it is not possible to observe the picking process in real time. As a consequence, the area of the preselected nanodiamond has to be scanned after every pick-up attempt, which is prohibitively time consuming and therefore was not further pursued after initial trials.

In the following we detail the pick-and-place technique since it the key technique in this chapter. We also discuss the properties of the nano-manipulator and how we identify nanodiamonds suitable for pick-and-place transfer. The pick-and-place process itself is very fickle and difficult to execute correctly. We are grateful for the guidance and support provided by C. Pauly, group of F. Mücklich, Saarland University in addition to the nano-manipulator setup itself.

1.1.1 Nano-manipulator

The nano-manipulator used for our experiments (Kleindiek, model MM3A-EM) has a exchangeable tungsten tip mounted inside a Thermo Scientific™ Helios NanoLab™ DualBeam™ microscope. This device combines a focussed ion beam and an electron microscope. The bent nano-manipulator tip can bee seen in Figure ?? has 3 degrees of freedom: up/down and left/right both in an arc up to 240°, and 12 mm in/out.

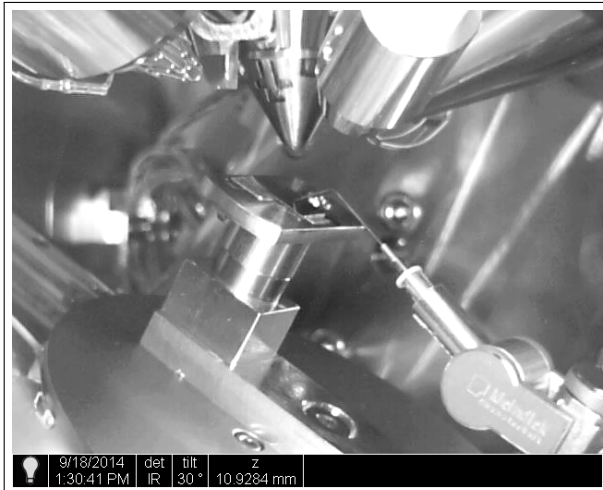


Figure 1.1: Image of the nano-manipulator mounted in the FIB. The arrows indicate the degrees of freedom of motion of the nano-manipulator. The custom made workbench is situated in the middle of the picture. On top of it, there is a 1 cm^2 substrate with coated nanodiamonds, the nano-manipulator tip pointing to the middle of it. Behind it, there is the target vertical-cavity surface emitting laser. Perpendicular to the workbench, the objective of the electron microscope can be seen. The angled cone perpendicular to the top edge of the image is the objective of the focussed ion beam.

Before using the nano-manipulator, its tip was “sharpened” with a focused ion beam

by etching away tungsten with gallium ions. Its final radius of curvature amounts to 100 nm. The sharpening enables the pick-up of nanodiamonds of a size suitable for use with photonic structures. In Figure 1.2a two sharpened tips are shown.

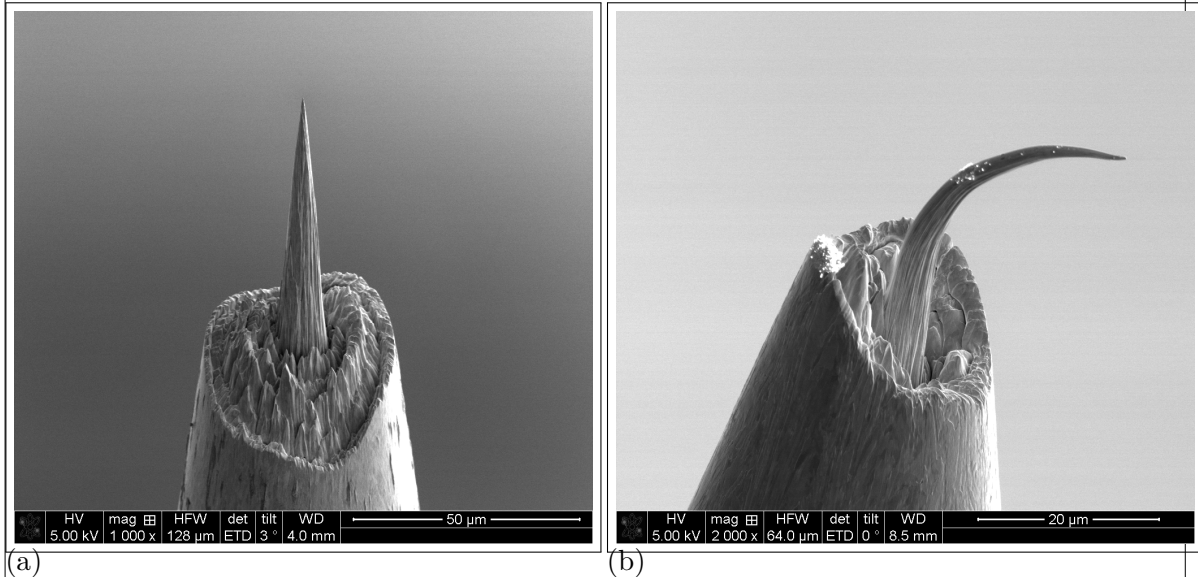


Figure 1.2: Detail of tips used as nano-manipulators. The actual tip can be seen projecting out from a bigger supporting structure. (a) Well-formed tip after sharpening. (b) Bend tip, silently attesting to the use of excessive force.

1.1.2 Determination of The Position of Nanodiamonds

Using the confocal setup detailed in ?? we identified nanodiamonds containing SiV centers suitable for the use in photonic structures. However, to actually move those nanodiamonds to a target photonic structure the SEM setup described in the previous section must be used. This implies that after substrates containing suitable nanodiamonds are mounted in the SEM setup, the same nanodiamonds must be located on the substrate in order for the nano-manipulator to address them correctly. To facilitate this and help locate relevant nanodiamonds, $10 \mu\text{m}^2$ cross markers with a nominal depth of 40 nm were milled into the iridium coating of the silicon substrate using the focussed ion beam prior to spin-coating the substrate with nanodiamond solution. The markers were arranged in a regular 11×11 grid covering an area of $0.5 \text{ mm} \times 0.5 \text{ mm}$. Figure 1.3a illustrates a sample array. Typically three arrays of markers were milled per substrate used.

To record the position of a nanodiamond with respect to a cross marker, we used two different methods:

In the first method the confocal setup is used with a white light source illuminates the sample from the side at an acute angle. As a result, the edges of the cross markers become visible in the fluorescence light scan, see Figure 1.3b. After turning the white

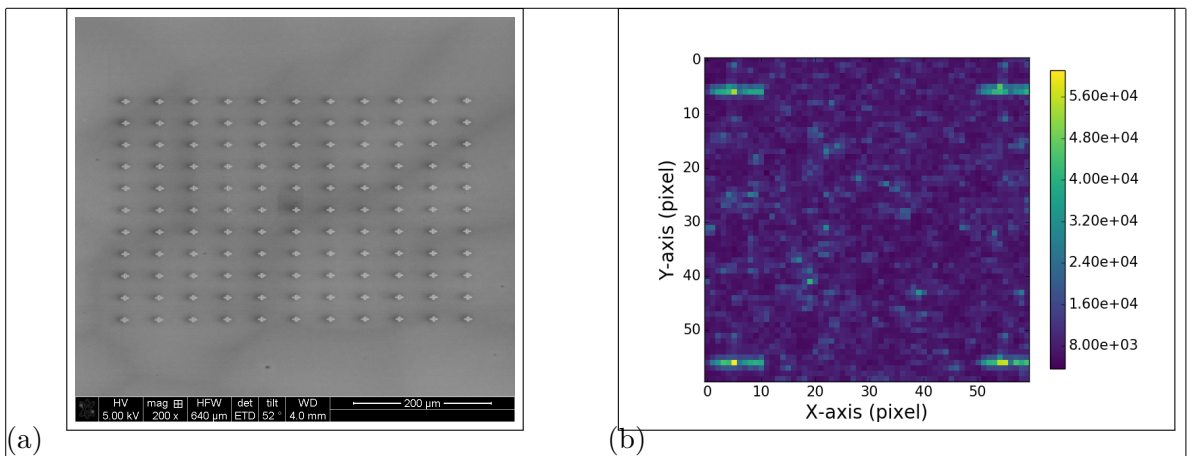


Figure 1.3: (a) Top-view of a regular array of cross markers. (b) White light scan of an area. Cross markers can be seen in all four corners.

light lamp off, the same area is scanned again to record the fluorescence from the SiV centers. An overlay of the two images identifies the position of fluorescent SiV centers with respect to the cross markers. The disadvantage of this method is the increased time consumption, as every scan for every subregion of the sample has to be performed twice. As only fluorescence light scans are performed, no information about the size of individual nanodiamonds is available. Furthermore, it remains unknown whether nanodiamonds are present in isolation or close to each other. Such information is only available in the SEM where the pick-and-place is conducted. It is only at this later stage, that individual nanodiamonds can be excluded as unusable for the pick-and-place process. For such nanodiamonds the time spend of characterizing its properties was unfortunately wasted.

To mitigate this problem, a more efficient method consists of scanning the substrate first using a commercial laser scanning microscope. The laser scanning microscope is a confocal microscope where the focus of a laser can be used to obtain the height of a structure. When scanning an array of cross markers a gray-scale image is obtained, where the gray value corresponds to the height deviation of a structure. As a result, both the crosses with a nominal depth of 40 nm and the nanodiamonds themselves are revealed as darker shades of gray. In contrast to the previous method, information on the size and isolation of nanodiamonds is accessible. After scanning the substrate with the laser scanning microscope, it is inserted into the confocal setup. While observing the surface with a CCD camera, a specific cross marker is chosen as the starting point for a fluorescence light scan. Comparing the laser scanning microscope image and a fluorescence light scan, fluorescent dots of the fluorescence light scan can be attributed to nanodiamonds in the laser scanning microscope scan. ?? illustrate the process.

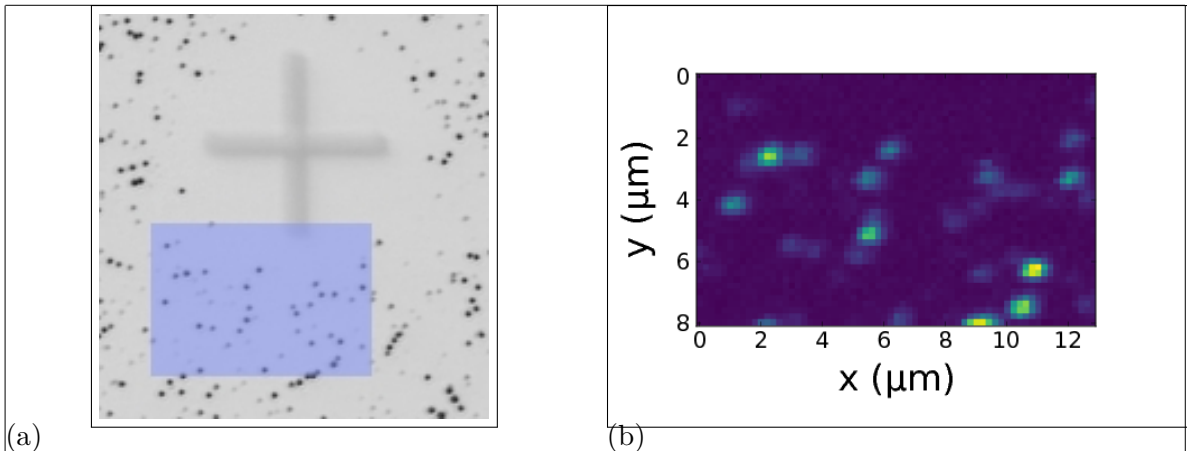


Figure 1.4: a) Picture recorded with a commercial high resolution laser scanning microscope. Cross marker is visible as well. b) Photoluminescence scan of a $8 \mu\text{m} \times 13 \mu\text{m}$ corresponding to the blue shaded area in b). The area shaded in blue represents the photoluminescence scan in image b).

1.1.3 The Pick-And-Place Process

The pick-and-place process aims to transfer a select nanodiamond between two substrates using the tip mounted inside a scanning electron microscopy. The advantage of using the SEM tip as a nano-manipulator lies in the fact that the progress of the manipulation process can be visualized directly, allowing for a better control of the operation. Figure 1.5 illustrates the process.

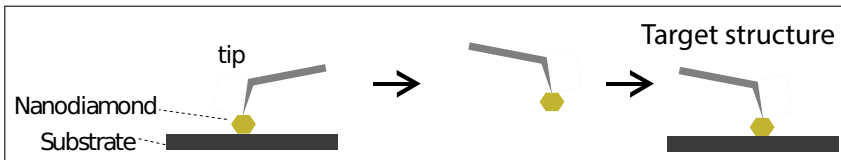


Figure 1.5: Sketch of the pick-and-place process

After we identified nanodiamonds as well-suited for transfer to the target structure, both the substrate with the nanodiamonds and the target structure were mounted inside the SEM. The process was performed using a high resolution mode with a low acceleration voltage of the SEM of 1 keV and a current of 1.7 nA. The tip is approaching the target preselected nanodiamond from above. As the SEM objective is mounted above the nanomanipulator, the proximity the nanomanipulator tip to the nanodiamond is not observable. To enable the tip of the nano-manipulator to pick up a target nanodiamond a precise approach is necessary. To facilitate this difficult procedure, the approach is divided into two stages: A coarse stage and a fine stage.

In the coarse stage the distance between tip and target nanodiamond is indirectly estimated from the shadow the tip itself casts onto the substrate and the focus area. As the tip approaches the target, the shadow of the tip starts to coincide with the nanodi-

amond position. At this point the fine stage of the approach begins in order to cover the remaining distance. To precisely control the final approach the focus of the SEM is used. Note that, as the distance between the tip and the target decreases, the focus must become sharp. Note that if the SEM is focused on the nanodiamond, the tip is out of focus and appears blurry. However, as the distance between the tip and the target decreases, the focus must become sharp. Thus the tip must be moved with utmost care until the focus becomes sharp at which point the tip touches the nanodiamond and pick-up can commence. While the process appears straightforward in concept, it is extremely challenging to operate the involved machinery to the required precision. As can be seen in Figure 1.2b it is easy to overshoot the target and to ruin the tip in the process.

When performed correctly, the nanodiamond sticks to the tip due to adhesion when the both get in contact, see Figure 1.6a. The nano-manipulator is then moved to the target structure and the approach procedure is applied in reverse. Figure 1.6b illustrates the tip of the nano-manipulator carrying a nanodiamond towards its destination structure. Depending on the material of the target structure, the nanodiamond either sticks to the structure right away due to higher adhesion forces between the nanodiamond and the structure (as is the case for golden plasmonic antennas). Alternatively, a sideways motion of the nanomanipulator tip must be used in an attempt to strike-off the nanodiamond. Either way, with patience it is possible to place a nanodiamond in a target position within a precision of a few nanometers.

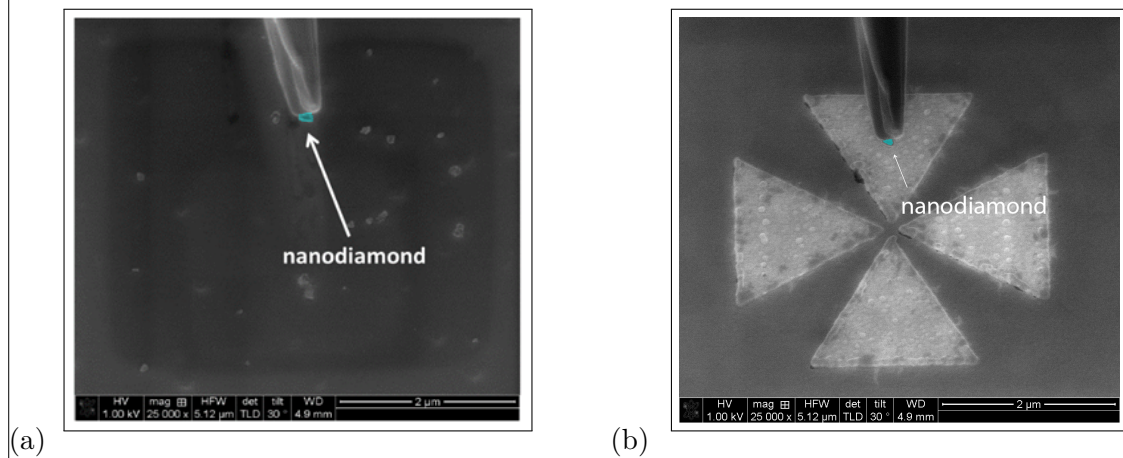


Figure 1.6: a) Tip of the nano-manipulator after successful pick-up of a nanodiamond. b) Tip of the loaded nano-manipulator approaching the target structure about to deliver a nanodiamond.

1.2 Coupling SiV centers to Vertical-Cavity Surface Emitting Lasers

In the context of metrology, controllable single photon sources, operating at room temperature, are an extremely important prospect. Such devices are anticipated to play a key role in the development and calibration of detectors and measurement methods aiming to resolve optical flux down to single-photon resolution [?]. As such single photon source form a cornerstone of the efforts directed towards the redefinition of the candela in terms of single photons, see discussion in ??.

Here we attempt to create a hybrid-integrated single photon source by placing a nanodiamond ideally containing a solitary SiV centers on-top of a vertical-cavity surface emitting lasers (VCSELs). The SiV center is situated such that output laser of the VCSEL can be used to optically excite the color center. Since the VCSEL laser can be controlled very well, SiV center operation can be steered reliably. Through the use of suitable optical filters allowing only SiV center fluorescence light to emerge, a controlled single photon source can be realized in principle.

In the following we give a short discussion of VCSELs. Next we discuss the coupling of SiV centers to VCSELs and report on the optical properties of the resulting hybrid-integrated light source.

1.2.1 Vertical-Cavity Surface Emitting Lasers

A vertical-cavity surface emitting laser is a type of semi-conductor laser diode [?, ?, ?]. Figure 1.7 illustrates a common design consisting of a p -layer on top and a n -layer at the bottom separated by a so-called active area. When a current is applied across the device, charge carriers migrate towards the active region. Holes act as charge carriers in the p region, whilst electrons carry charge in the n -region. The material properties of the active region is chosen such that when electrons and holes spontaneously recombine, a photon is emitted in the process. Electron-hole pairs can also dissipated via the creation of phonons leading to losses in the form of heat. To define the region for recombination to occur and to control the optical properties of the device, additional thin layers of semi-conducting material can be introduced in the active area. These result in the formation of quantum wells with associated energy levels and resulting preferred transitions with well-defined energies for the recombination of electrons and holes.

To achieve lasing, stimulated recombination and thus stimulated emission of photons is required. To facilitate this both p -region and n -region are constructed in a layered fashion allowing them to act as highly-efficient distributed Bragg reflectors (DBR). Thus the active region is sandwiched by two mirrors forming the resonator of the laser diode. Spontaneously emitted photons thus are temporarily trapped continuously interacting with the active region. Provided the presence of sufficient electron-hole pairs, a photon

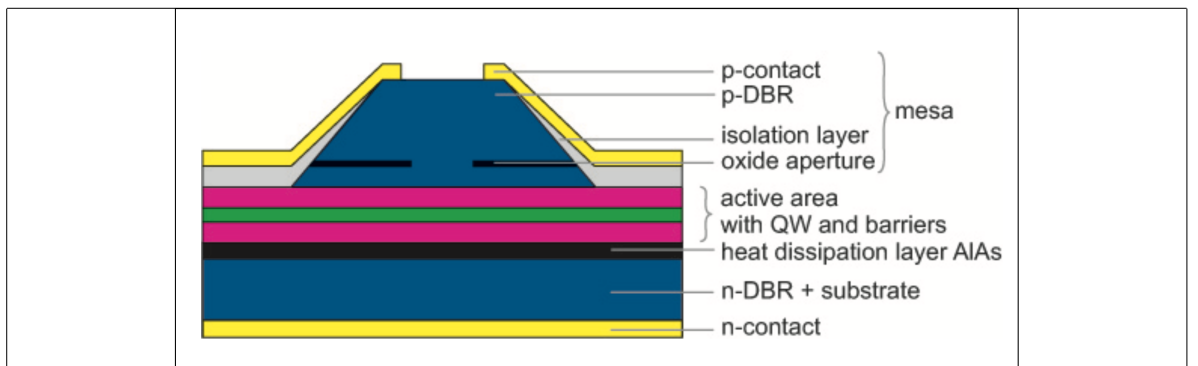


Figure 1.7: Illustration of a VCSEL laser diode [?]. When a current is applied across the device via contacts (yellow), holes and electrons migrate from the *p*-region (blue, top) and the *n*-region (blue, bottom) towards the active region (purple+green, center) where they recombine emitting photons. A quantum well is inserted in the active region, shaping the recombination process. *p*-region and *n*-region are acting as DBRs forming the resonator of the laser. When enough photons are gained by via stimulated emission, a laser beam emerges from the *p*-region after passing an oxide aperture.

can stimulate their recombination and thus the emission of further identical photons which themselves increase the stimulated emission. If enough identical photons are gained in this process, a coherent laser beam is formed by the fraction of photons escaping the resonator through the *p*-region. As a result the laser beam produced by a VCSEL is perpendicular to the substrate it resided on.

VCSELs have a range of properties that make them particularly interesting for industrial applications such low power consumption, ease of fabrication and cheap production. As a result, VCSELs are utilized in a broad range of applications including fiber optic communications or precision sensing and are used widely in commonly encountered devices such as computer mice or laser printers [?].

In the context of this thesis VCSELs offer several advantages. Their output beam is perpendicular to the substrate surface and suitable to excite SiV centers. This means that nanodiamonds containing SiV centers can simply be placed onto the device. Furthermore their physical size is ideal for the nanodiamonds we work with. The small size of VCSELs will make it easier to deploy the resulting hybrid-integrated light sources in future applications.

1.2.2 SiV center in a Vertical-Cavity Surface Emitting Laser

Remark:

Gegeben einen nanodiamond ist es ja a priori unwahrscheinlich, dass ein einziges SiV center drin vorkommt. In antenneteil gehen wir darauf ein. Hier nicht. Warum nicht? Auch im Siv paper ist keine thematisierung.

To conduct our research, we received an array of red AlGaInP-based oxide-confined VCSELs from P. Michler, Stuttgart University. The array includes three individually operable VCSELs, two of which, labeled VCSEL Bm4 and VCSEL Bm2 were used in our experiments, see Figure 1.8a.

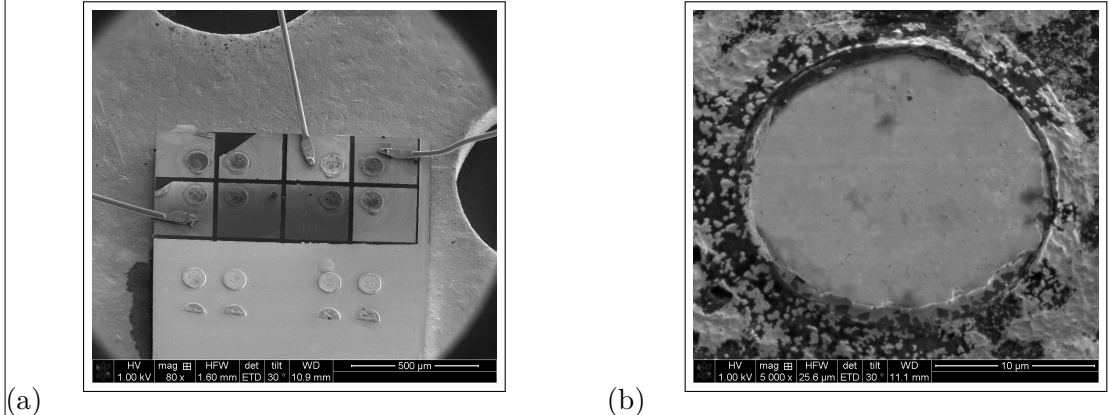


Figure 1.8: (a) SEM image of an array of VCSELs. The three wires are the anodes, which are connected to the top layer (*p*-contact) of the VCSEL. Therefore, three of the VCSEL structures can be operated. VCSEL Bm4 is located in the top right while VCSEL Bm2 to the left of it. (b) Detail SEM image of the top of VCSEL Bm4. The circular middle part is the hole in the *p*-contact through which the top DBR is visible. The smaller active diameter measures $5.8\text{ }\mu\text{m}$ through which the laser light exits the structure is not visible in the SEM. A successful pick-and-place operation positions a nanodiamond hosting an SiV center directly in the path of the VCSELs laser.

The VCSELs we obtained use a *n*-type DBR consisting of 50 pairs of AlAs/Al_{0.5}Ga_{0.5}As mirror pairs while the *p*-type DBR is formed by 36 Al_{0.95}Ga_{0.05}As/Al_{0.5}Ga_{0.5}As [?]. The active region itself consists of 4 GaInP quantum wells. An oxide aperture in a field node of the standing wave serves as a spatial filter for maximum modal gain by confining the current and the optical mode. The active diameter which is defined by the oxide aperture is $5.8\text{ }\mu\text{m}$.

The available VCSELs are perfect candidates for the excitation of SiV centers in a hybrid integrated single photon source for several reasons. They exhibit a circular beam profile, have low divergence angle and emit linearly polarized light. Their physical size and the fact, that their output beam is perpendicular to the substrate implies that our nanodiamonds containing nanodiamonds can simply be placed on-top of the structure light-emitting region using pick-and-place methods, see Figure 1.8b. Thus the VCSELs output laser can be used to optically excite SiV centers.

As a first step towards using VCSELs to excite color centers, we characterized the behavior of VCSEL Bm4. To this end we operated it at currents of 1.5 mA and 3 mA and recorded the resulting lasing wavelength. The emission spectra showed that the emitted continuous wave laser light to be around 655 nm in wavelength for both currents, see Figure 1.9a. Previous research within the authors group recorded SiV center intensity

maxima at excitation wavelengths of 720 nm and 680 nm [?], aligning reasonably well with the output wavelength of VCSEL Bm4.

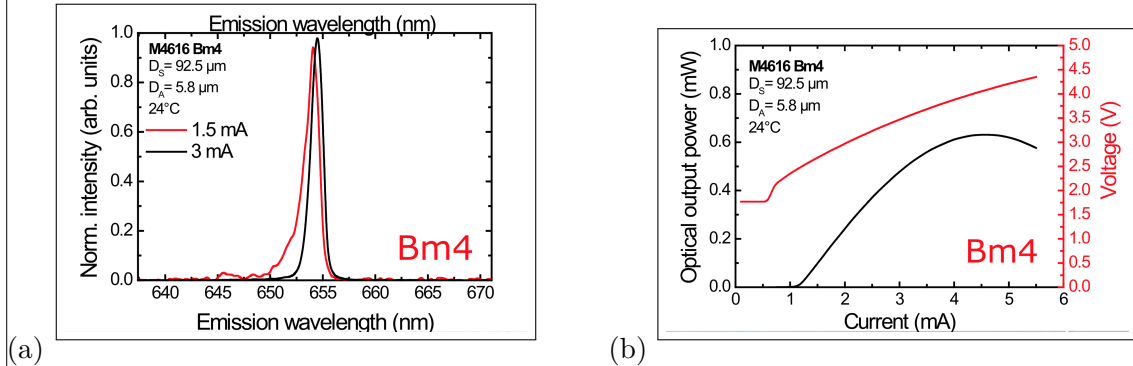


Figure 1.9: (a) Emission spectrum of VCSEL Bm4 at two different currents. (b) Optical output power and voltage of VCSEL Bm4 in dependence of input current. □

The optical output power of VCSEL Bm4 as a function of the current applied is given in Figure 1.9b. In addition, the resulting voltages are shown. It can be seen that the maximum power of ≈ 0.6 mW is reached for moderate currents of ≈ 4.5 mA. While the available optical powers are small comparable to using a conventional laser, low powers are sufficient for initial explorations.

The next step consists of selecting a suitable nanodiamond containing an SiV center followed by transferring it onto of VCSEL Bm4. To this end nanodiamonds 200 nm in size were grown with the CVD method in an iridium coated silicon wafer. We refer the reader to ?? for details on the process.

Next, using the confocal setup described in ?? a nanodiamond was identified exhibiting one dominant line at 746.0 nm with a linewidth of 1.9 nm. Its position on the substrate was determined consecutively using a white light laser scan as described in subsection 1.1.2. Given the position of the nanodiamond it was then transferred to VCSEL Bm4 and placed precisely in its active, i.e. light-emitting region. The process of introducing an SiV center to another structure is referred to as coupling.

After successful transfer VCSEL Bm4 was inserted into the confocal setup. Using the laser from the confocal setup we checked if the pick-and-place process caused any modification of the spectroscopic properties of the SiV center such as a decrease of count-rate or a modification of the fluorescence light spectrum. During these checks, the VCSEL itself was not active.

As a first check, we scanned the VCSEL surface in an attempt to detect the activity of the introduced SiV center. Figure 1.10a shows the SiV center as a bright dot in the aperture of VCSEL Bm4. For comparison, a Vertical-Cavity Surface Emitting Laser without coupled SiV center exhibits solely background counts which is shown in Figure 1.10b.

The spectrum of the SiV center in the transferred nanodiamond was investigated before and after the pick-and-place process. section 1.11 shows that the original spectrum

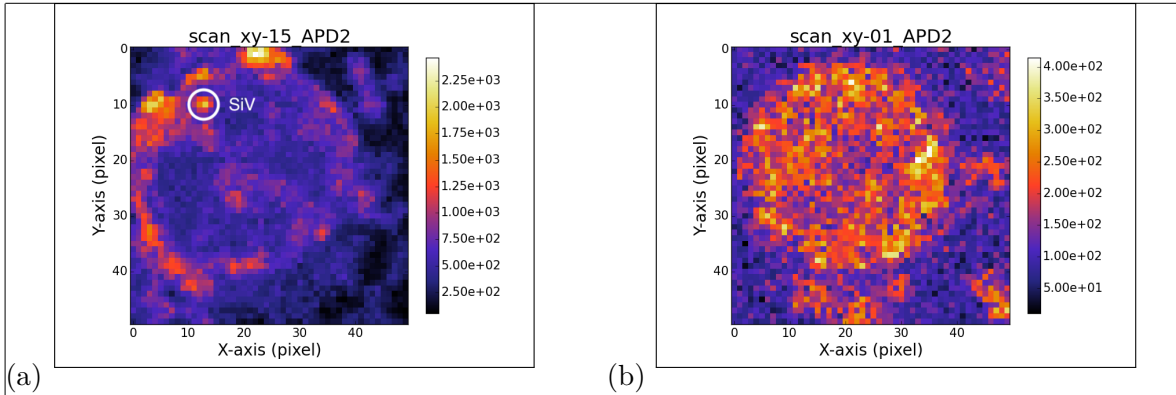


Figure 1.10: (a) Scan of the VCSEL Bm4 with coupled nanodiamond under excitation with the laser from the confocal setup. The big visible ring is the edge of the circular aperture in the *p*-contact of VCSEL Bm4. The bright spot in the upper left corner corresponds to the transferred nanodiamond containing an SiV center causing a spike in the count-rate. (b) Scan of the VCSEL Bm2 lacking a nanodiamond under excitation with the laser from the confocal setup. The circular aperture in the *p*-contact exhibits a constant count-rate. Note the different scales.

before nanodiamond transfer exhibits one dominant line at 746.0 nm, denoted line *A*. Furthermore, two minor peaks can be seen. The lower wavelength peak is denoted as line *B*. Interestingly, after the pick-and-place process, a different picture emerges shown in section 1.11. The once dominant line *A* is strongly reduced. The new dominant feature is line *B*. Note that the count rate of line *B* remained the same before and after pick-and-place.

The observed reduction of the intensity of line *A* is difficult to explain. One cause could be damage to the color center due to the electron radiation it was exposed to during the pick-and-place process. This is supported by previous research in this authors group recording reduced fluorescence light intensities after color centers were exposed to electron radiation [?]. However, the fact that line *B* remains virtually the same before and after pick-and-place is curious, raising the question whether damage alone is sufficient to explain the observed effect. As it stands, the question remains open and is thus subject to further investigation.

With line *B* as remaining dominant line we then operated VCSEL Bm4 at 1.84 mA and 3.3 V, turning off the laser of the confocal setup. Thus SiV center excitation is due to the output laser of VCSEL Bm4.

For comparison, we scanned both the surface of VCSEL Bm4 including a nanodiamond as well as VCSEL Bm2 without a nanodiamond. A bandpass filter allowing light between 730 nm to 750 nm to pass was used. This filter window suppresses the VCSEL laser line at 655 nm while leaving the SiV center emission nearly unchanged. The results of the two scans are given in Figure 1.12, where the bright areas correspond to the circular VCSEL output regions. It can be seen that no difference in brightness can be established between a VCSEL with and without a nanodiamond containing a SiV

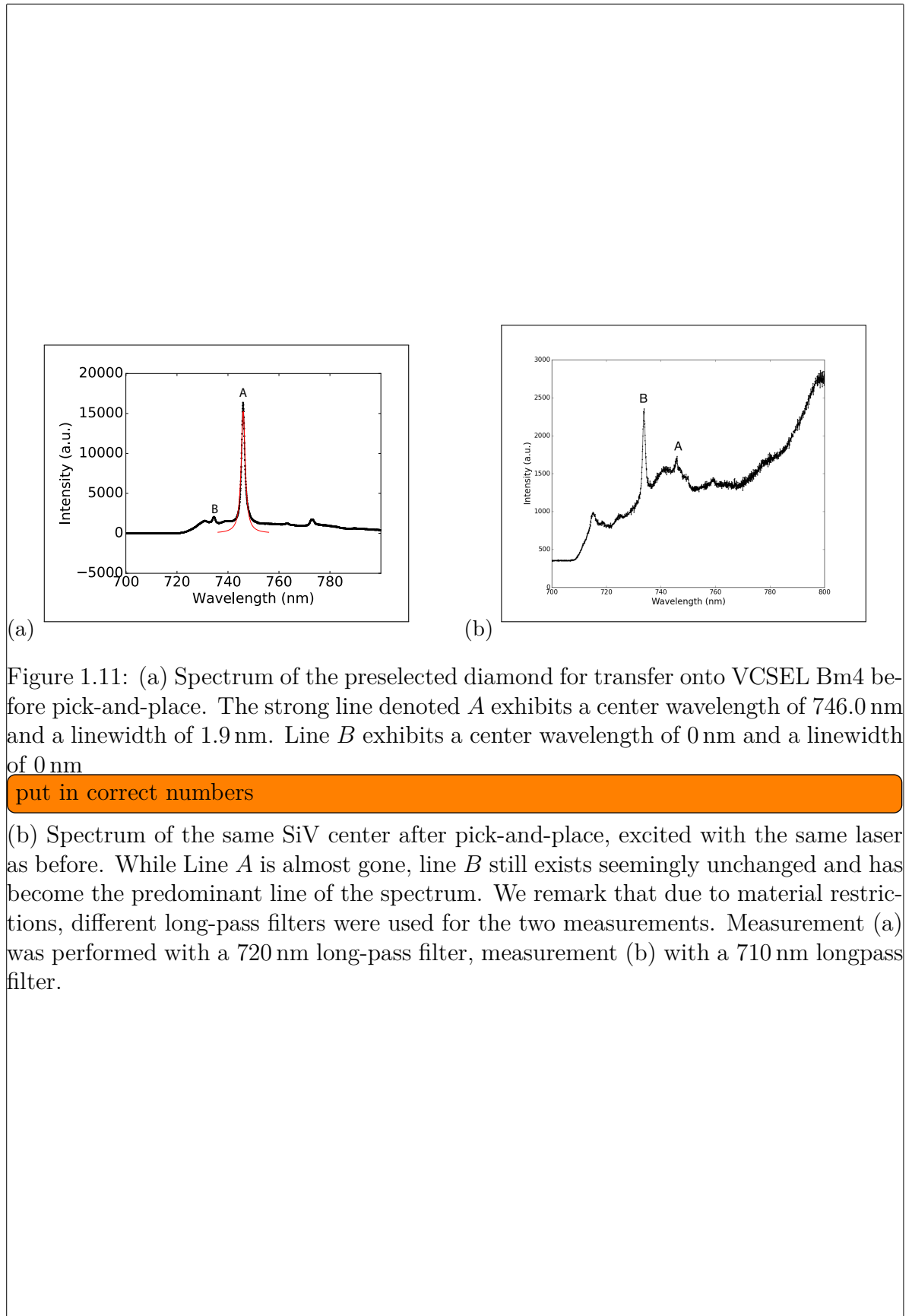


Figure 1.11: (a) Spectrum of the preselected diamond for transfer onto VCSEL Bm4 before pick-and-place. The strong line denoted *A* exhibits a center wavelength of 746.0 nm and a linewidth of 1.9 nm. Line *B* exhibits a center wavelength of 0 nm and a linewidth of 0 nm

put in correct numbers

(b) Spectrum of the same SiV center after pick-and-place, excited with the same laser as before. While Line *A* is almost gone, line *B* still exists seemingly unchanged and has become the predominant line of the spectrum. We remark that due to material restrictions, different long-pass filters were used for the two measurements. Measurement (a) was performed with a 720 nm long-pass filter, measurement (b) with a 710 nm longpass filter.

center.

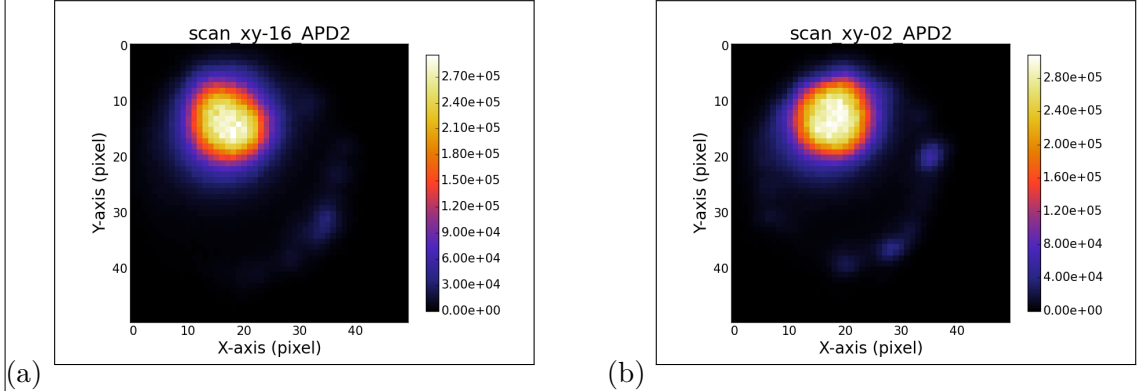


Figure 1.12: (a) Scan of the laser light stemming from VCSEL Bm4 and the fluorescence light from the SiV center in the filter window 730 nm to 750 nm. (b) Scan of the laser light stemming from VCSEL Bm2 without a coupled SiV center. The outcome of the two scans is almost identical.

To further investigate we conduct spectroscopic measurements. Since the position of the nanodiamond in VCSEL Bm4 is known, we measure the spectrum of light originating from this position. A second spectrum is obtained from VCSEL Bm2 measuring the corresponding position without a nanodiamond present. Figure 1.13 reports the results. Again no meaningful difference between the two VCSELs can be established. The lack of any distinct lines in the spectrum taken for VCSEL Bm4 which can be attributed to SiV center emission is striking.

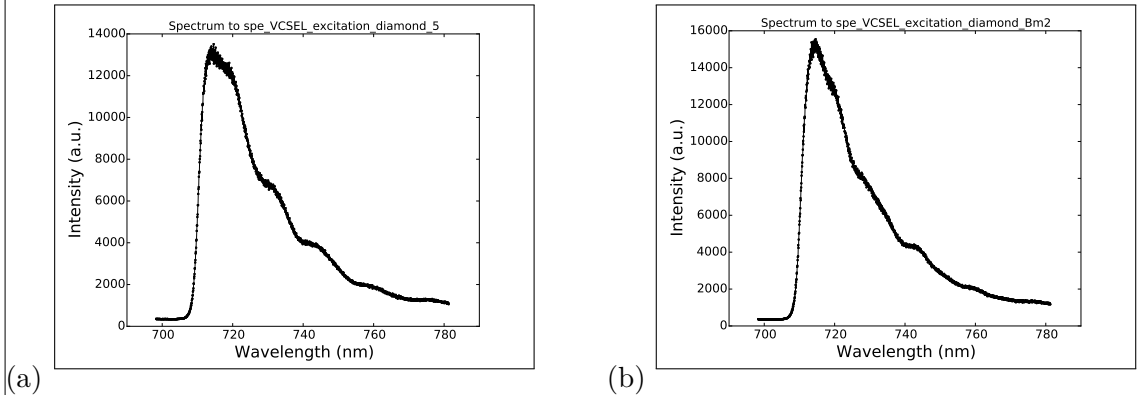


Figure 1.13: (a) Recorded Spectrum of the SiV center in the transferred nanodiamond coupled to VCSEL Bm4 during VCSEL operation. No distinct SiV center lines are visible. (b) Recorded spectrum of VCSEL Bm2.

To explain the observation, the following considerations are reasonable: The SiV center is excited by the VCSELs laser and thus emitting single photons which are passing through the filter window. The same is true for photons stemming from VCSEL side band emission. Given that the emission from the side band of VCSEL Bm4 dwarfs the

single photon emission of its SiV center, the obtained results are reasonable. To confirm we examine the reflectivity of the DBR of VCSEL Bm4. section 1.14 illustrates that the DBR exhibits imperfect reflexivity in the wavelength region relevant for SiV center emission. As a result, relevant side band emissions of VCSEL Bm4 are not sufficiently suppressed to allow for SiV center emission to be detected. This in turn means that our initial attempt to realize a hybrid-integrated single photon source by coupling an SiV center to a VCSELs is thwarted by large side band emissions of the latter.

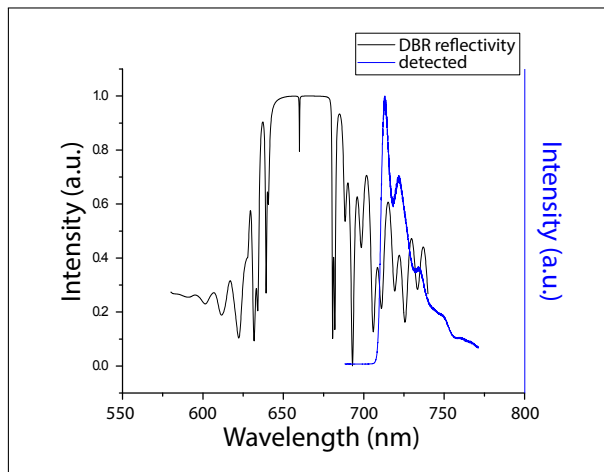


Figure 1.14: Reflectivity of the Distributed Bragg reflector (DBR) of VCSEL Bm4 [?], and a spectrum of the SiV center measured during VCSEL excitation for comparison. The reflectivity of the DBR and the VCSEL emission spectra are depicted with different scales. The shape of the measurement of the SiV center during VCSEL operation is reminiscent of the shape of the DBR reflectivity. The spectrum of the SiV center is not visible. As the emission from the SiV center is small compared to the intensity of the laser side band in the same wavelength regime, the SiV centers emission is not detectable

warum schaut das spectrum anders aus als das, was einzeln geplottet ist?

Despite a failed first attempt, a clear direction for further improvement was identified, i.e. focusing on ways to reduce VCSEL side band emission in the relevant SiV center emission regime. A promising approach to suppress the side band is to add a gold layer on top of the VCSEL acting as an additional mirror. While films of gold have a transmittance maximum at 500 nm, the transmittance minimum depends on the film's thickness [?]. Thus a gold layer could in principle be used to suppress the VCSEL side band in the SiV center emission regime. Provided such a layer can be engineered and is effective, one may expect SiV center emission to be recovered. Efforts in this direction are a required next step towards the realization of hybrid-integrated single photon sources based on SiV centers coupled to VCSELs.

1.3 Coupling Nanodiamonds to Double Bowtie Antenna Structures

Plasmonic nano-antennas are very recent devices designed to efficiently convert freely propagating optical radiation into localized energy and vice versa [?, ?, ?, ?, ?, ?]. Leveraging this unique property, integrating SiV centers with optical antennas creates coupled systems with a range of desirable features. These include enhanced photoluminescence emission and the ability to tailor photoluminescence spectra of the integrated emitters. The latter can be achieved by tuning the physical design parameters of the system including antenna geometry and emitter placement.

In this chapter we report on our efforts aimed at enhancing the properties of SiV centers by coupling them to optical double bowtie antennas. To this end we transfer selected nanodiamonds containing SiV centers to the target antenna structure using pick-and-place methods. After successful coupling we investigate the integrated structure experimentally. In addition to that we successfully relate some of our results to theoretical predictions.

In the following we give a short discussion of the most important properties of optical antennas. Then we sketch the actual coupling process and report on the optical properties of the resulting integrated structure. To our knowledge, our experiments were the first attempts of coupling SiV centers to plasmonic bowtie antennas.

1.3.1 Plasmonic Antennas

Optical nano-antennas act as converters between propagating and localized electromagnetic fields. Thus, they can be used efficiently to couple photons in and out of nano-scale objects [?]. Due to their small physical sizes, comparable or smaller than the wavelength of visible light, they are capable of focusing optical fields to sub-diffraction-limited volumes, offering the ability to manipulate electromagnetic fields at nano-scales [?, ?]. This property, dubbed sub-wavelength confinement, has successfully been exploited to enhance the excitation and emission of quantum emitters [?, ?, ?, ?] and to modify their spectra [?]. Resulting practical applications include near-field optical microscopy [?], surface enhanced spectroscopy [?, ?] and molecular sensing [?].

A nano-antenna is a nano-structure made from materials such as noble metals like gold or silver. These metals have in common that they are very susceptible to being polarized by electro-magnetic fields. When illuminated by the incident electromagnetic radiation causes electrons in the metal to behave as a plasma that tends to move with respect to the atomic lattice. As a result excess charge at the opposite surfaces of the material accumulates and the material becomes temporarily polarized until restoring forces equilibrate the charge distribution.

Thus incident light of a given frequency induces oscillations in the free electron gas density in the surface layers of the metal. At resonance these light-induced oscillations

exhibit modes of standing waves. The quasi-particles associated with these modes are known as localized surface plasmons (LSPs). For an in-depth treatment of LSPs in the context of nano-antennas we refer the reader to [?] and references therein.

Here it suffices to say, that LSPs facilitate the deciding property of optical antennas: Converting electromagnetic energy from the far-field into localized energy in the near-field. This allows, in combination with the high collection-efficiencies of nano-antennas, to efficiently couple visible radiation with wavelengths of hundreds of nanometers, into small effective spatial volumes of only a few nanometer in diameter.

To create a controlled hot-spot several antenna designs are possible. In the context of this thesis we rely on double bowtie antennas available via a collaboration with N. Rahbany, group of C. Couteau, University of Technology of Troyes. Figure 1.15 illustrates the typical bowtie antenna.

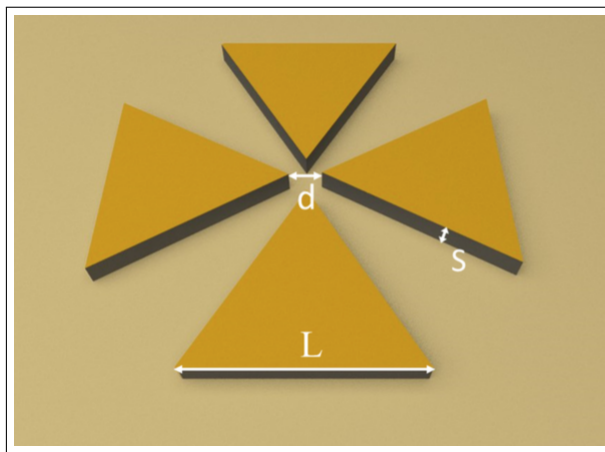


Figure 1.15: Schematic of a double bowtie antenna [?, ?, ?].

This antenna design utilizing a symmetric arrangement of four identical triangle-shaped blocks, separated by a small gap. This setup allows LSP modes local to individual blocks to couple with each other resulting in the formation of an intense hot-spot in the center area [?], see ?. The actual electromagnetic response of a double bowtie nano-antenna depends on its physical design parameters such as gap size, material used, geometry and size. Furthermore, properties of incident light such as wavelength and polarization determine antenna operation.

The improved electromagnetic field at the center of a metallic nano-antenna can be used to increase the spontaneous emission rate of emitters emitting at frequencies close to the resonance frequency of the antenna. This result is the known as Purcell effect [?]. The gap between the antenna arms acts as a resonant cavity providing a strong near field interaction with the emitter. This interaction modifies the density of states of the system, effectively providing additional modes for the emitter to decay into, thus amplifying its total decay rate. The amplification affects both radiative and non-radiative decay. The magnitude of the amplification for an emitter is quantified by the ratio of its enhanced decay rate to its free space decay rate, known as the Purcell

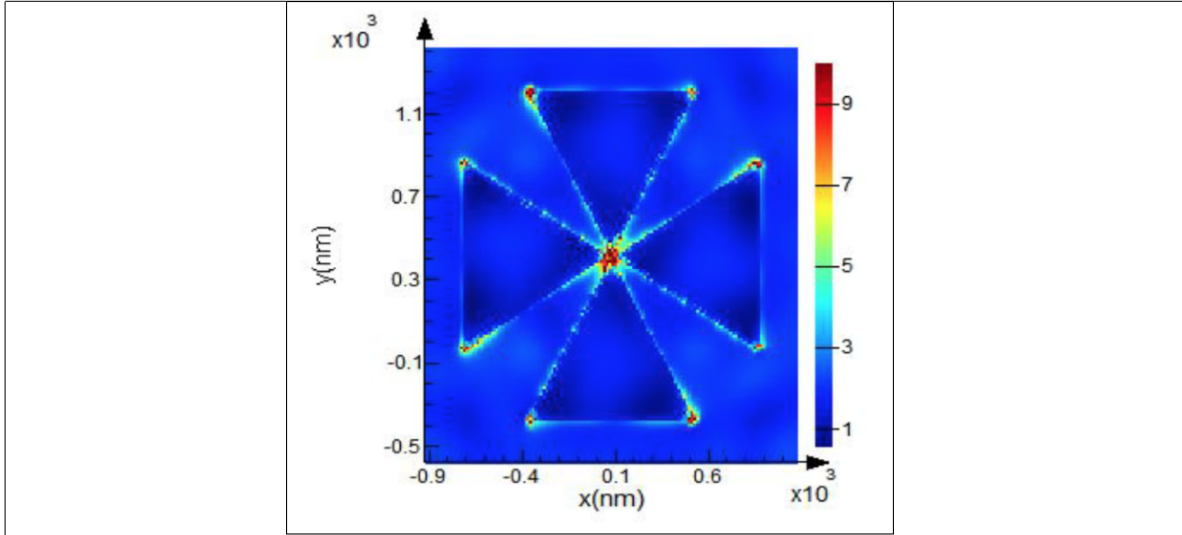


Figure 1.16: Simulation result of the electric field map of a gold double bowtie nanoantenna [?, ?, ?]. The structure has gap of $d = 150$ nm, a side length of $L = 2\text{ }\mu\text{m}$ and a thickness of $S = 60$ nm. The center of the antenna exhibits an area of pronounced focus, the so-called hot-spot.

factor F_p . This factor is proportional to Q/V_{eff} where Q denotes the quality of the antenna and V_{eff} the volume of the hot-spot. Thus antenna design must optimize F_p as a necessary condition for significant enhancement of fluorescence light emission.

In addition to the antennas local field enhancement, the emitters original quantum yield η_0 influences the overall effectiveness of the emission enhancement. From theoretical considerations [?, ?, ?, ?], the modified quantum efficiency η of the combined system consisting of emitter and antenna can be obtained as

$$\eta = \frac{\eta_0}{\frac{1-\eta_0}{F_p} + \frac{\eta_0}{\eta_{ant}}}, \quad (1.1)$$

where η_{ant} denotes the fraction of fluorescence light which is not dissipated through losses in the metal of the antenna. It is clear that an emitter with $\eta_0 \rightarrow 1$ will not profit from the Purcell effect. On the contrary, for realistic antennas with $\eta_{ant} < 1$ antenna-induced losses reduce the overall quantum yield η . Consequently poor emitters with low initial η_0 stand to profit the most from antenna-emitter coupling provided antennas are engineered well, i.e. they maximize their Purcell Factors and minimize their losses. For an in-depth review

The presented considerations illustrate that due to their relatively low quantum efficiency, SiV centers are excellent candidates for coupling with antennas. Thus it is promising to exploit the improved electromagnetic field at the center of a double bowtie antenna to enhance the spontaneous emission rate of SiV centers and thus improve their merit as single photon sources.

1.3.2 Plasmonic Antenna Design and Simulation

To couple SiV centers to optical antennas, we work with gold double bowtie antennas on a gold substrate. In comparison with triangular, or single bowtie antennas, double bowtie antennas offer significantly improved intensity enhancements. Antennas were provided by N. Rahbany, group of C. Couteau, University of Technology of Troyes in a joined effort to explore the possibilities of combining antennas with SiV centers. The antennas themselves were fabricated using electron beam lithography, a technique suitable to imprint predetermined patterns onto a suitable substrate with nano-scale resolution [?]. Figure 1.17a shows a SEM image of an array of antenna structures of various sizes. In Figure 1.17b a detail of an individual double bowtie antenna is shown. It can be seen that the double bowtie antenna is placed in the center of another structure, a so-called bulls-eye antenna, consisting of multiple concentric gratings. When illuminated by a laser at a proper angle, the gratings excite surface plasmon polaritons (SPPs) which are directed towards the center of the structure. If a double bowtie antenna is present in the center, SPPs can interact with the LSPs of the double bow tie, leading to an even stronger localization of electromagnetic fields in the gap of the bowtie. While this interaction certainly merits exploration in the context of enhancing SiV centers, we omit the excitation of SPPs in our first exploration of the coupling of SiV centers and antennas. Thus the presence of the gratings can be ignored for our purposes. The reader interested in the details of bulls-eye antennas and their properties is referred to [?].

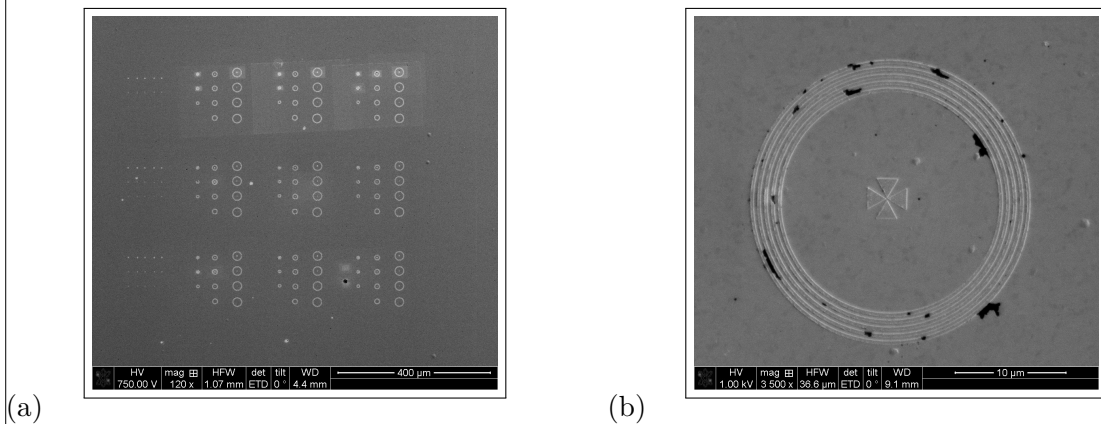


Figure 1.17: SEM images of antenna structures. (a) Overview of a field of antenna structures exhibiting various dimensions. (b) Detail of one antenna structure. In the middle the double bowtie design is visible. A grating structure consisting of multiple gratings is surrounding it.

To effectively enhance the emission of an emitter by coupling it to an optical antenna, the emission wavelength must match the resonant wavelength of the antenna. In the context of SiV centers a value of 738 nm is required. Since this value can be considered constant, the design parameters of the antenna must be chosen such, that the resulting resonance matches it. An additional constraint is placed on the size of the antenna gap,

since it must be big enough to accommodate nanodiamonds hosting SiV centers, the former are around 100 nm in size. However, it cannot be chosen arbitrarily big, since bigger gaps lead to larger effective volumes and thus smaller Purcell Factors.

Using finite time difference domain (FDTD) simulation deploying Lumerical Software the design space of gold double bowtie nano-antennas on a gold substrate was explored [?]. Although we initially attempted to simulate antennas without a nanodiamond present in the gap, it was subsequently discovered that its ab initio inclusion yielded superior results. Thus to determine usable design parameters for our purposes, an integrated system combining antenna and nanodiamond was used. To better mimic experimental conditions and associated imperfections, the nanodiamond was placed slightly off-center in the gap.

In a series of simulation it was established that a gap-size of $d = 150$ nm, a side length of $L = 2\text{ }\mu\text{m}$ and a structure thickness of $S = 60$ nm are feasible parameters as referred to in ???. The simulation required the index of refraction for gold which was taken from Palik [?, ?, ?, ?].

The resulting geometry hosting a nanodiamond is capable of producing a suitable hot-spot when excited.

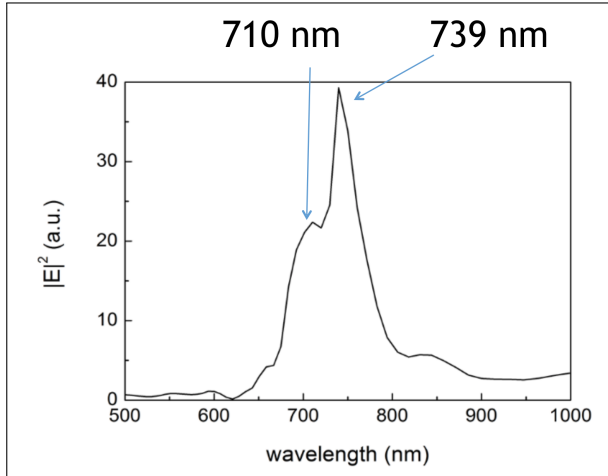


Figure 1.18: FDTD simulation of the electric field intensity of a double bowtie nano-antenna as a function of the wavelength of incident light. Two peaks are identified. The major peak corresponds exceptionally well with SiV center emission at 738 nm. The minor peak is attributed to the presence of a nanodiamond.

Finally, to pin-point the resonant wavelength for the antenna hosting a nanodiamond, the electric field intensity is simulated as a function of the wavelength of the incident light. The resulting spectrum is shown in Figure 1.18. Two resonant peaks are found. The intense major peak at 739 nm coincides exceptionally well with the SiV center emission wavelength 738 nm indicating successful antenna design. In addition to the major peak, an additional minor mode at a lower wavelength of 710 nm is found [?]. We remark that if the nanodiamond in the gap of the antenna is removed from the

simulations, the minor feature vanishes. Thus the additional peak is well-attributed to the presence of the nanodiamond.

In summary, the combined simulation results suggest, that the engineered system of nano-antenna and nanodiamond is well suited to effectively enhance the emission from an SiV center hosted in the nanodiamond. In the following sections we report on the experimental realization of this preposition.

1.3.3 SiV center in a Plasmonic Double Bowtie Antenna

In the following we report on our attempts to couple SiV centers to gold double bowtie nano-antennas in order to study the properties of the resulting integrated system. Ideally, a suitable nanodiamond containing exactly one SiV center is placed in the center of the antenna. The term suitable is used to summarize both desirable spectroscopic properties such as narrow-bandwidth saturated single-photon emission as well as technical requirements such as nanodiamond size and degree of isolation on the surface. Naturally, the odds of identifying and addressing a nanodiamond fulfilling all these criteria simultaneously are small. As a result identifying a perfect candidate for coupling is prohibitively time-consuming.

To mitigate this difficulty we decided to relax the condition of exactly one SiV center per nanodiamond and initiate our exploratory work with nanodiamonds containing several, potentially many active SiV centers. Relying on $g^{(2)}(0)$ measurements we identify two interesting classes of nanodiamonds. The first class consists of nanodiamonds containing large ensembles of SiV centers acting as coherent emitters. The fluorescence light received from large ensemble of emitters is mainly coherent, leading to a flat response in the $g^{(2)}(0)$ function. The second class of nanodiamonds we investigate features nanodiamonds hosting multiple SiV centers. As a result relevant $g^{(2)}(0)$ measurements report weak but discernible anti-bunching dips. Both classes have in common that relevant nanodiamond specimen are significantly easier to obtain than nanodiamonds containing singleton SiV centers. Thus nanodiamonds containing ensembles of SiV centers as well as nanodiamonds containing few SiV centers are both valid starting points for our work. It is likely that the experience gained during our preliminary explorations will be valuable once nanodiamonds containing singleton SiV centers become available.

In the following sections we report on our efforts to couple nanodiamonds containing SiV centers to antennas. We illustrate the coupling process and its challenges and discuss relevant results regarding the coupling of nanodiamonds of the classes described above. We close the chapter with a short discussion and suggestions for further research.

Nanodiamonds Containing Ensembles of SiV centers Coupled to Antennas

Remark:

- fuer Figure 1.20b braucht noch das richtige bild. also eine g2 function mit coherent light
- die photostrecke pick-and-place kannst du noch nancy bilder durch deine bilder ersetzen. Ansosten muessen da noch nancy citate hin.

The nanodiamonds used for the approach of coupling ensembles of SiV centers to an antenna were wet-milled from a CVD diamond film¹. The solution of nanodiamonds exhibiting a median size of 100 nm was spin-coated on an iridium substrate treated with Piranha etch. To ensure that a preselected nano-diamond exhibiting preferred optical properties can reliably be located, the iridium substrate was engraved with reference cross markers produced by a focused ion beam after the spin-coating process. After spin-coating, the sample was placed in an oven for 3 h at 450 °C to oxidize the surface and remove any residual graphite and amorphous carbon. See ?? for more information.

To determine the position of nanodiamonds on the original substrate, first a scan with a commercial laser scanning microscope (LSM) was performed as described in subsection 1.1.2. Figure 1.19a shows a part of an obtained LSM image. After transferring the sample into the confocal setup, confocal fluorescence light scans of the corresponding areas are performed to identify nanodiamonds containing active emitters. The scanned area is shown in Figure 1.19b. It corresponds to the area shaded blue in Figure 1.19a. Thus, upon close inspection some of the bright spots appearing in the fluorescence light scan can be associated with selected nanodiamonds in Figure 1.19a by eye. The correspondence between the SEM and LSM images in conjunction with the cross-markers on the substrates allows to precisely locate preselected nanodiamonds containing suitable emitter in the SEM.

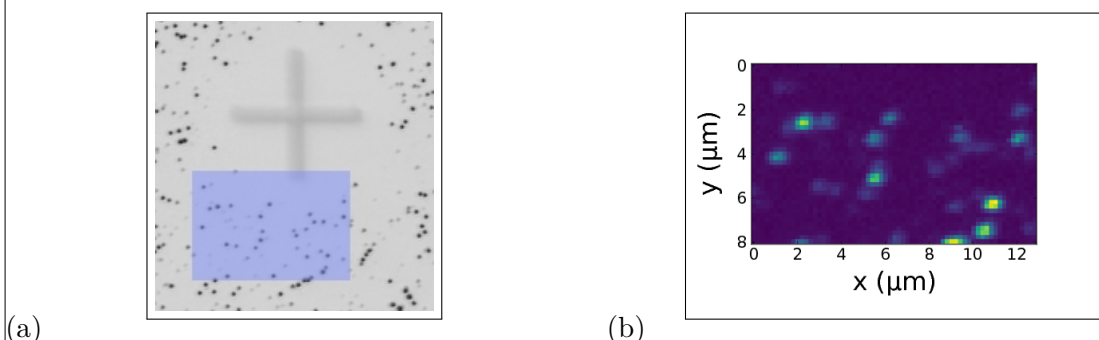


Figure 1.19: (a) Picture recorded with a commercial high resolution laser scanning microscope. Black dots are individual nanodiamonds. The cross-marker serves as an orientation aid. The area shaded in blue represents the photoluminescence scan in image (b). (b) Photoluminescence scan of a $8 \mu\text{m} \times 13 \mu\text{m}$.

The most promising candidate nanodiamonds are characterized by fluorescence light

¹wet-milling performed by A. Muzha, group of A. Krueger, Julius-Maximilians Universität Würzburg, diamond film grown by group of O. Williams, School of Engineering, Cardiff University

spectra with very narrow zero-phonon-lines and minimal phonon side band features. Figure 1.20a shows the spectrum stemming from one such preselected nanodiamond. The ZPL feature exhibits a center wavelength of (738.55 ± 0.01) nm and a linewidth of (5.00 ± 0.03) nm, corresponding well with the ZPL of unstrained SiV centers. Photon autocorrelation measurements revealed that the nanodiamond contains an ensemble of SiV centers collectively generating coherent fluorescence light light, see Figure 1.20b.

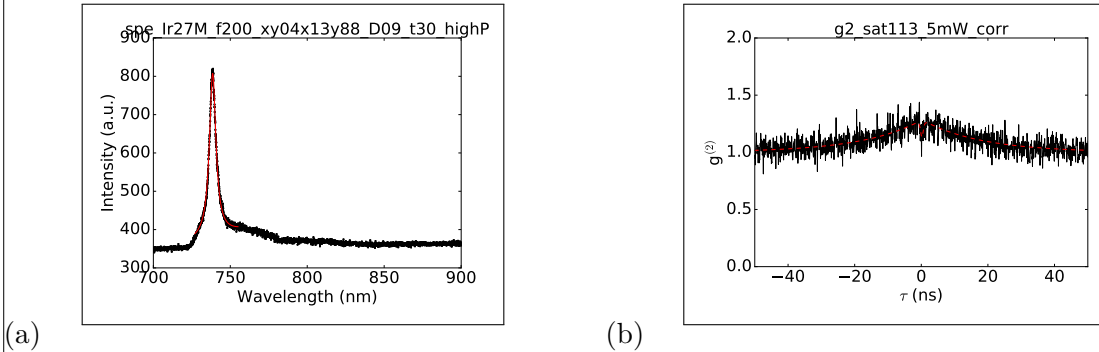


Figure 1.20: a) PL spectrum of the emitter in the preselected nanodiamond at room temperature. Black: experimental results; red: fit to experimental data, which yields a ZPL center wavelength of (738.55 ± 0.01) nm and a linewidth of (5.00 ± 0.03) nm. b) Intensity autocorrelation function recorded for the ensemble of emitters hosted by the nanodiamond. The flat response indicates the coherent nature of the fluorescence light light.

After a proper candidate for coupling with an antenna has been identified, it needs to be relocated from its original substrate to the antenna. To this end a pick-and-place process introduced in subsection 1.2.1 is used. A complete illustration of the steps involved is given in Figure 1.21.

We remark that the gold surface of the plasmonic antenna exhibited strong adhesion forces between the antenna surface and the nanodiamond. Once the nanodiamond touched the gold, it could not be picked up again with the tungsten tip. The nanodiamond first touched the antenna structure a few nanometers away from the gap and immediately stucked to the surface, on top of one of the triangles. Therefore, the nanodiamond had to be pushed into the gap with the nano-manipulator tip. This process caused some damage to the antenna structure. The damage is visible as black area at the tip of the top triangle in Figure 1.21e. Luckily, FDTD simulations of damaged antennas reveal that this modification of the antenna hardly influences the antenna resonance.

After successful placement, the antenna sample is installed in the confocal setup. The antenna itself was located during a scan of the sample surface under white light illumination. A scan of the antenna is performed in the confocal setup using a 660 nm continuous wave laser. It serves to locate the middle of the antenna structure and therefore the nanodiamond which had been placed there. An outline of the rings is visible in an overview scan of the antenna structure shown in Figure 1.22a. Zooming

1.3. COUPLING NANODIAMONDS TO DOPPLERLESS PHOTONIC STRUCTURES

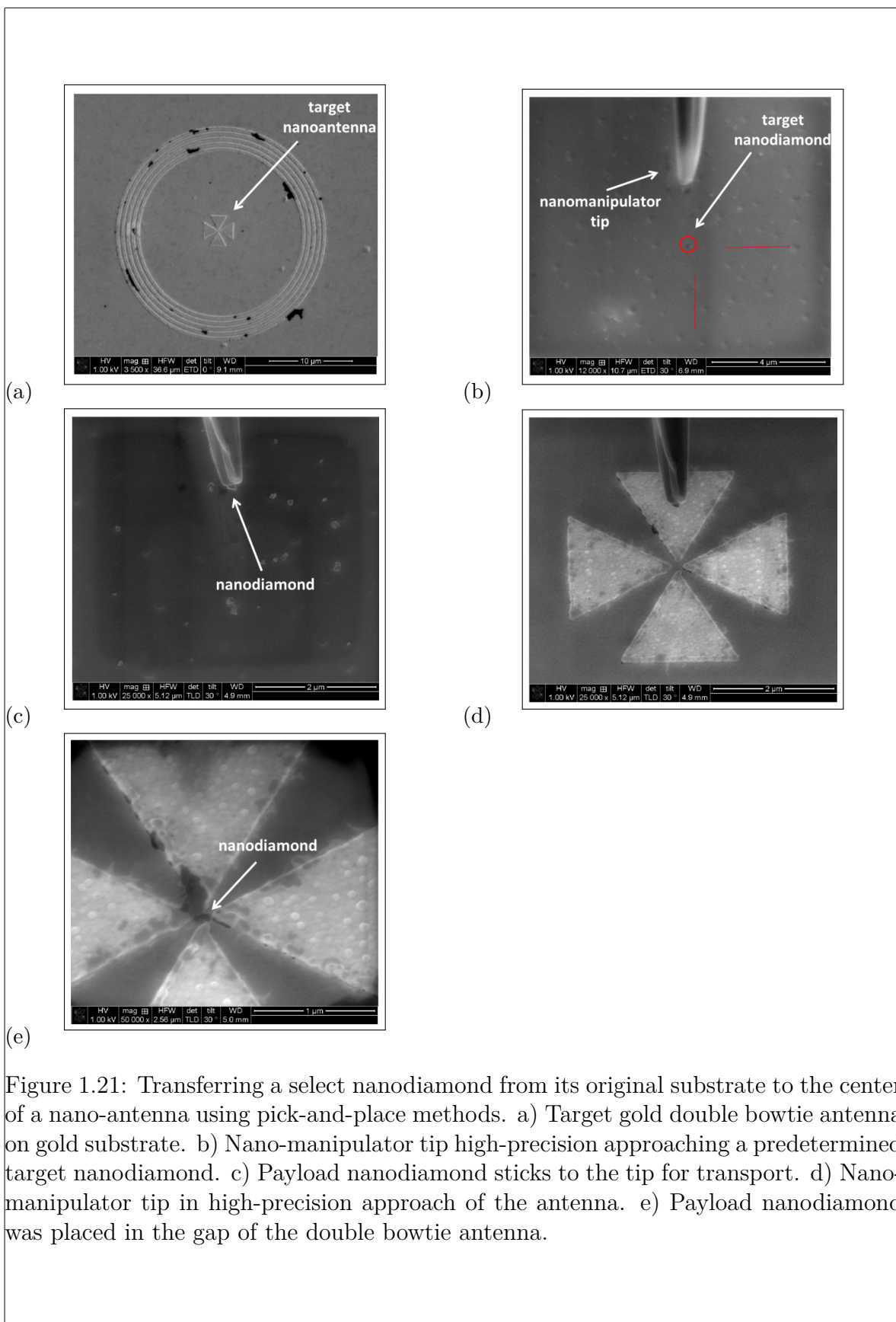


Figure 1.21: Transferring a select nanodiamond from its original substrate to the center of a nano-antenna using pick-and-place methods. a) Target gold double bowtie antenna on gold substrate. b) Nano-manipulator tip high-precision approaching a predetermined target nanodiamond. c) Payload nanodiamond sticks to the tip for transport. d) Nano-manipulator tip in high-precision approach of the antenna. e) Payload nanodiamond was placed in the gap of the double bowtie antenna.

in to the exact center of the rings, some of the edges of the bowtie antenna are vaguely visible in Figure 1.22b.

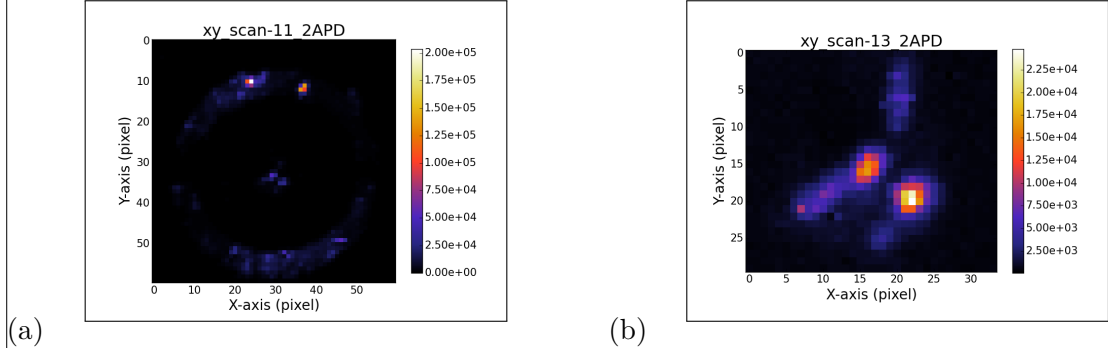


Figure 1.22: (a) Confocal scan of the double bowtie antenna where a nanodiamond containing multiple SiV centers had been placed. The rings are visible. (b) Detail scan of the triangles of the same antenna structure, which make up the double bowtie antenna. While the separate triangle cannot be seen, some edges and two bright spots are visible. To identify the place of the nanodiamond we compare the middle point of the rings in (a), the point of intersection of the edges and the bright spot and conclude that the upper bright spot in (b) is the location of the nanodiamond.

These images suffices to locate the nanodiamond with sufficient precision to measure PL spectra. The PL spectrum of the ensemble of SiV centers in the nanodiamond is shown in Figure 1.23a. It can be seen that at 738 nm a major peak is present, almost exactly at the same wavelength than the SiV center zero-phonon-line, i.e. 739 nm. The additional minor peak at 726 nm is attributed to the antenna resonance mode. We remark that, any damage sustained through electron radiation during the pick-and-place process is likely not sufficient to invalidate the nanodiamond. This is expected as a large ensemble of SiV centers can easily lose several emitters without any noticeable difference in the optical properties. Needless to say, the exact opposite is true for nanodiamonds with very few hosted SiV centers making them risky to work with.

We verified successful coupling of the ensemble of SiV centers to the antenna by combining experimental and numerical results. In particular, we convolve the experimental PL spectrum of the nanodiamond measured before placing it in the nano-antenna, see Figure 1.20a, with the intensity spectrum of the nano-antenna obtained by means of simulations given in ???. The result of the convolution is the spectrum given in Figure 1.23b. The agreement with the measured spectrum in Figure 1.23a is almost perfect, indicating successful coupling of emitters and antenna. At the same time we confirm that the minor peak in Figure 1.23a is indeed due to the antenna resonance.

Finally, keeping experimental conditions unchanged, we measure a spectrum of an identical antenna without a nanodiamond present in order to rule out surprising artifacts induced by the antenna itself. The resulting spectrum is given in Figure 1.24.

At this point one must resist the temptation of comparing the values of the intensity maxima of the spectra in Figure 1.20a and Figure 1.23a in order to determine the

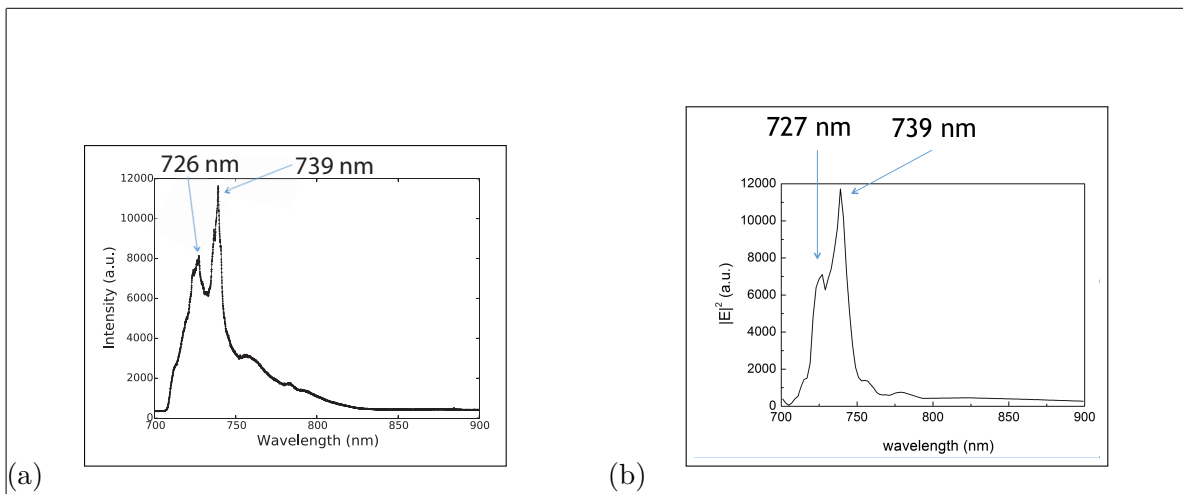


Figure 1.23: (a) Measured PL spectrum of the emitter after placing the nanodiamond into the nano-antenna, (b) Convolution of the spectrum of the measured PL spectrum of the emitter before pick-and-place, see Figure 1.20a, and the simulated resonance spectrum of the nano-antenna, see Figure 1.23a.

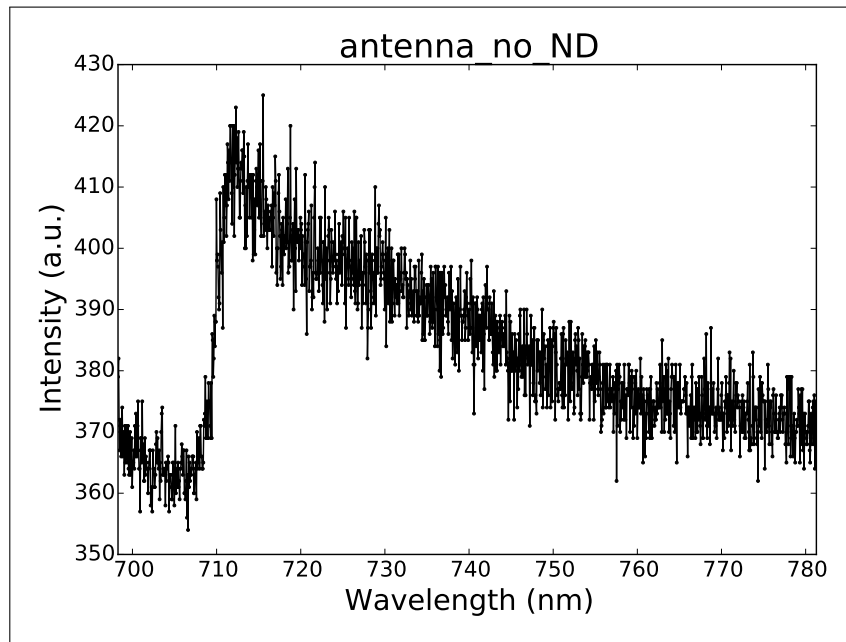


Figure 1.24: Spectrum of a gold double bowtie nano-antenna without a nanodiamond present.

enhancement the ensemble of emitters experiences. These values inherently do not allow a meaningful comparison.

A meaningful comparison can in principle be achieved via intensity saturation measurements. By measuring the saturation intensities before and after insertion into the antenna and accounting for effects related to the polarization of emitters, the magnitude of the Purcell enhancement can be determined. Unfortunately, these methods are reserved for single emitters and do not apply for ensembles of SiV centers. Thus at this point we have no method to determine the Purcell enhancement ensembles of SiV centers experience.

In summary, in this section we showed that coupling of nanodiamonds containing ensembles of SiV centers with gold double bowtie antennas is feasible using a pick-and-place approach. Furthermore we verified that the coupling is indeed present after the nanodiamond was placed in the gap of the antenna. Unfortunately, at present there is no reliable method available to us to quantify the magnitude of fluorescence light enhancement experienced by the SiV center ensemble.

Nanodiamonds Containing Few SiV centers Coupled to Antennas

Remark:

- FDTD bilder fehlen komplett. Muessen unten eingefuegt werden.
- FDTD simulation fuer verschiedenen dipole orientations werden kurz erwaehnt, gibts da bilder?
- Fuer das spectrum von nanodiamond + antenne sind die locations von den subpeaks wichtig? Irgendwo sollte erwaehnt werden, dass der neue major peak nicht dort ist wo man die SiV center zero-phonon-line erwarten wuerde.
- Die fits an die subpeaks von dem spectrum nanodiamond + antenne werden nicht erklaert. Wenn die nicht wichtig sind, sollte man sie zumindest beilaeufig erwaehnen.

After a first successful validation of inserting nanodiamonds hosting large ensembles of SiV centers into a gold double bowtie antenna, we attempt to select nanodiamonds containing a comparatively small number of SiV centers. Suitable nanodiamonds show an anti-bunching dip in the $g^{(2)}$ function in addition to count-rate saturation. This can be regarded an intermediate step towards using nanodiamonds containing singleton SiV centers. We stress that in comparison to nanodiamonds hosting large ensembles of emitters, nanodiamonds containing only a few emitters are already difficult to identify. Naturally, technical requirements applying to candidate nanodiamonds such as sufficiently isolation for picking it up in the pick-and-place process and a size not larger than that of the antenna gap still need to be observed.

The starting material for the nanodiamonds used here was an electronic grade diamond film produced by the company rho-BeSt coating (now renamed to CarbonCompetence).

The film was then milled in a bead-assisted sonic disintegration process² to nanodiamonds of a median size of approximately 100 nm. The nanodiamonds were drop-cast at 60 °C onto an iridium substrate containing cross markers. Prior to drop-casting the substrate was cleaned with Piranha etch.

Given samples containing nanodiamonds the tedious task of identifying potential candidates for transfer to the antenna. As described in the previous section, a commercial laser scanning microscope (LSM) is used to identify nanodiamonds on the substrate. Using the cross markers to address their exact positions, a corresponding fluorescence light scan allow us to single out nanodiamonds with bright emission. We further test the suitability of potential candidates as follows. First, a saturation curve is recorded to establish whether the SiV centers in a nanodiamond saturate. Since saturation is a necessary albeit not sufficient condition for single-photon emission, only nanodiamonds that saturate are capable of showing an anti-bunching dip in the $g^{(2)}$ function. Note that, measuring the $g^{(2)}$ function potentially requires hour-long measurements, while determining saturation requires merely seconds. Thus, in search of candidate nanodiamonds we may use the saturation behavior as a quick check whether a candidate is feasible to follow up with a lengthy $g^{(2)}$ function measurement. For nanodiamonds containing SiV centers showing saturation we then check the spectrum to assert that the emitters are indeed SiV centers. After this last check $g^{(2)}$ function measurements are established.

After a significant search, involving a sizable number of discarded candidates, a nanodiamond with a discernible anti-bunching dip was found. ?? shows its $g^{(2)}$ function function while Figure 1.25b reports its saturation curve. While the dip in $g^{(2)}$ function is quite weak, it is present and a fitting it was possible. This indicates that the nanodiamond neither contains a singleton SiV center nor does it host enough SiV centers to emit coherent light. Thus we conclude that a limited number of SiV centers must be present. While it is not possible to quantify the number of emitters directly, the candidate sufficiently differs from nanodiamonds hosting large ensembles of SiV centers. Thus it is viable to take it to the stage of coupling.

In order to relocate the identified nanodiamond to the center of a gold double bowtie antenna we repeat the pick-and-place procedure described in the previous section, see Figure 1.21. We remark at this point that since the nanodiamond in question contains fewer SiV centers as compared to the nanodiamonds hosting large ensembles of SiV centers, it is expected to be less resilient to adverse effects such as the electron radiation present during the pick-and-place process.

After a successful relocation, the sample containing the antenna is mounted in the confocal setup to investigate the properties of the combined system consisting of antenna and SiV centers. Figure 1.26a gives the spectrum of the candidate nanodiamond after being relocated to the center of a gold double bowtie antenna. Interestingly we find a multitude of individual peaks in the vicinity of the SiV center zero-phonon-line line. In addition we find that the sideband appears more pronounced in relation to the intensity

²A. Krueger, Julius-Maximilians Universität Würzburg

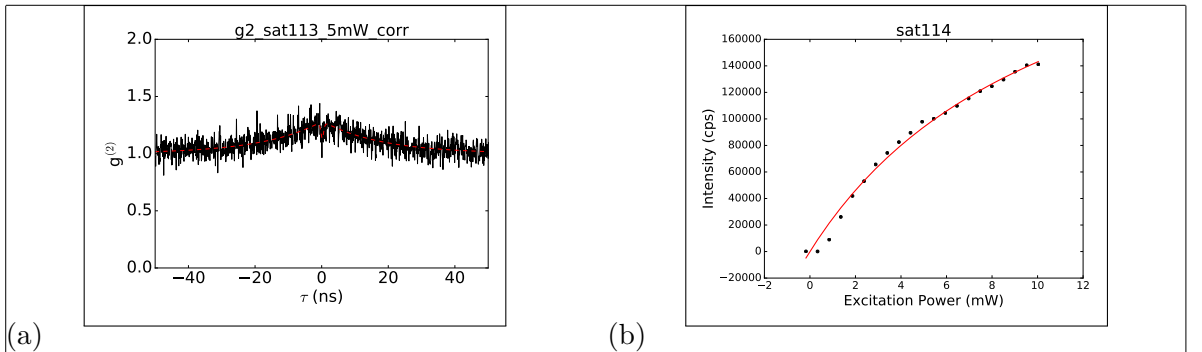


Figure 1.25: (a) The $g^{(2)}$ function of the preselected nanodiamond believed to host a limited number of SiV centers. A dip at $g^{(2)}(0)$ is present, however its decrease is not sufficient for a singleton SiV center. This indicates that a limited number of SiV centers is present since the absence of a dip can only be measured under coherent emission, i.e. for larger ensembles of SiV centers. The dashed red line gives a fit to the data.

cps zu a.u. aendern

. (b) Saturation curve of the same emitter

zahlen fuer sat eintragen

. Data points are black, fitted curve red.

of the major feature after the nanodiamond has been relocated to the antenna. Due to the shape of the recorded sideband we conjecture that it arises as a combination of the phonon side bands associated with individual SiV centers and additional contributions due to fluorescent contaminations. Figure 1.26b showing the spectrum of the same nanodiamond before being relocated to the antenna. Here the phonon side band is weaker in comparison to the zero-phonon-line feature.

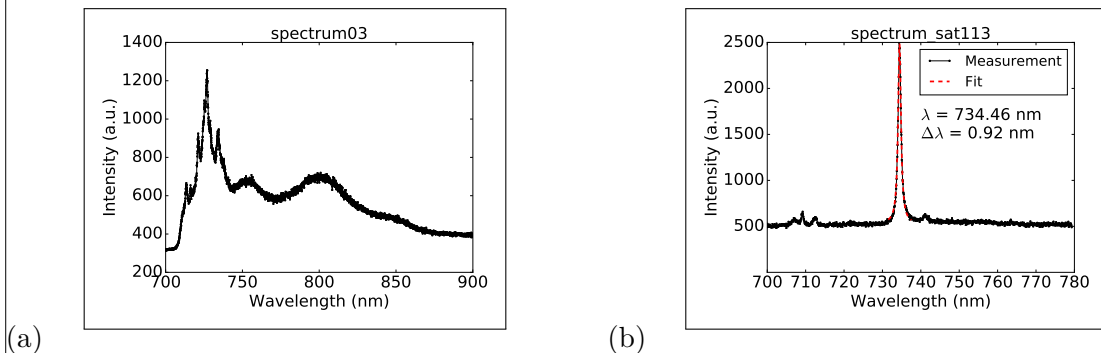


Figure 1.26: (a) Spectrum of the preselected nanodiamond hosting few SiV centers after being relocated to the center of a double bowtie antenna. (b) Spectrum of the same nanodiamond before relocation.

To exclude the possibility that the obtained peaks are artifacts due to misalignment of the experimental setup, we rechecked the alignment which proved to be precise.

To reverify the obtained spectrum, we repeated the measurement. Unfortunately, we

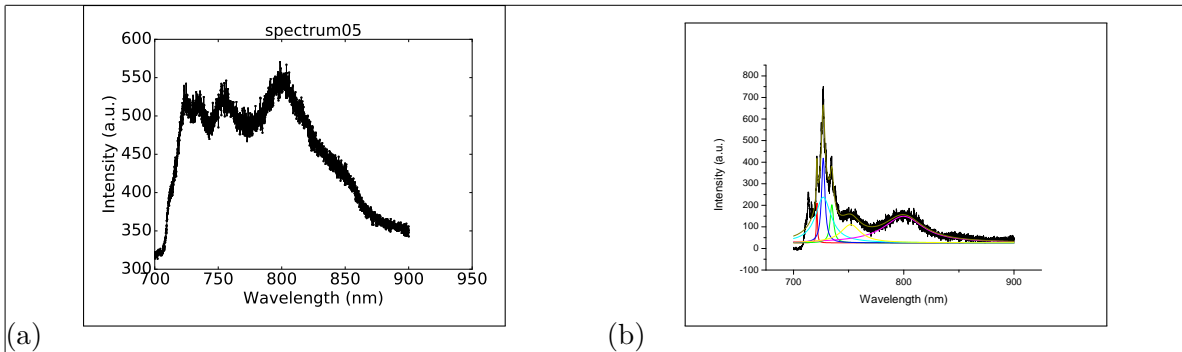


Figure 1.27: (a) Spectrum of the nanodiamond hosting few SiV centers coupled to the double bowtie antenna after the emitter bleached. (b) Background corrected spectrum of the transferred nanodiamond in the double bowtie antenna. Peaks are fitted, results of the fits are the colored lines. For background correction, the spectrum in (a) was used.

obtained an entirely different result, showing only a broad background seen in Figure 1.27a. After checking in the confocal scan that the measurement was performed at the correct position, we had to conclude that all of the SiV centers hosted by the nanodiamond permanently bleached after recording the spectrum seen in Figure 1.26a. It is likely that continued application of energy from the laser triggered this effect as earlier independent measurements established that SiV centers exhibit an increased likelihood of bleaching after being exposed to electron radiation [1]. Thus we conclude that the exposure to electron radiation during the pick-and-place left the SiV centers in an unstable state susceptible to bleaching.

Even though the nanodiamond was invalidated for further measurements, the spectrum that was obtained remains to be discussed further. To better understand the obtained observations, we turn to FDTD calculations of nanodiamond coupled to a gold plasmonic double bowtie antenna as described in the beginning of this chapter. In particular, we fold the spectrum of the nanodiamond before insertion into the antenna as given in Figure 1.26b with the simulation spectrum of the integrated system consisting of nanodiamond and antenna. The simulation result thus constitutes a prediction of what we the spectrum in Figure 1.26a should look like. ?? illustrates the simulation prediction and demonstrates that we have no reason to expect the to see the peaks between 700 nm to 750 nm observed experimentally. Hence we must conclude that the spectrum of the nanodiamond was modified during the pick-and-place process. While it is not possible to pinpoint exactly which circumstance caused the modification, several effects could influence the observed spectra.

First, the electron radiation itself. While it lacks the energy to modify the lattice itself, it can influence the electrons present and in particular may modify the charge state of SiV centers. As was mentioned before, electron radiation was linked to increased likelihood of photo-bleaching.

Next, during the pick-and-place process it is possible that the nanodiamond collects

additional contaminating matter on its surface. Contaminations may be fluorescing themselves, thus modifying the spectrum. The fact that we record a significant sideband signal in Figure 1.26a supports this conjecture.

Yet another property of SiV centers which should not be neglected is their dipole orientation interacting with the antenna. Conducting dedicated FDTD simulations with a focus on different dipole orientations indicated a dramatic effect on the resulting spectra. Therefore, future experiments aiming to investigate the effect of coupling nanodiamonds containing few SiV centers to antennas should include polarization measurements to experimentally quantify the impact of the emitter orientation.

As it stands, the most likely explanation of the recorded spectrum consists of a combination of the discussed effects. Since the nanodiamond bleached almost immediately no further measurements were possible. It is thus advised to repeat the experiment hoping for a nanodiamond that manages to complete the pick-and-place process unharmed. At the moment it is not clear if this can be done, thus further investigation is required.